INTERNATIONAL JOURNAL OF HYDROGEN ENERGY 39 (2014) 8293–8302

Available online at www.sciencedirect.com

ScienceDirect

journal homepage: www.elsevier.com/locate/he

Phase boundary of pressure-induced *I4mm* to *Cmc2*$_1$ transition in ammonia borane at elevated temperature determined using Raman spectroscopy

Yongzhou Sun [a], *Jiuhua Chen* [a,b,*], *Vadym Drozd* [a], *Andriy Durigin* [a], *Shah Najiba* [a], *Xiaoyang Liu* [b]

[a] *Center for the Study of Matter at Extreme Condition, Department of Mechanical and Materials Engineering, Florida International University, Miami, FL 33199, USA*

[b] *Center for High Pressure Science and Technology Advanced Research, Jilin University, Changchun 120013, China*

ARTICLE INFO

Article history:
Received 24 December 2013
Received in revised form
5 March 2014
Accepted 12 March 2014
Available online 24 April 2014

Keywords:
Ammonia borane
Hydrogen storage
Raman spectroscopy
Clapeyron-slope
Pressure-induced phase transition

ABSTRACT

The pressure-induced tetragonal (*I4mm*) to orthorhombic (*Cmc2*$_1$) phase transition in ammonia borane has been studied in a diamond anvil cell (DAC) using *in situ* Raman spectroscopy. At near ambient pressure in DAC, ammonia borane started decomposing as low as ~88 °C, but at higher pressure, ammonia borane is stable up to 100 °C above 0.5 GPa. In the pressure–temperature phase diagram, the boundary between tetragonal (*I4mm*) and orthorhombic (*Cmc2*$_1$) phase was determined by the characteristic change in Raman spectra during compression and decompression at 3 constant temperatures: 20, 60 and 100 °C, respectively. The result shows that the phase transition is reversible with a small hysteresis, while the phase boundary shifts towards higher pressure with increasing temperature and a positive Clapeyron-slope. The positive Clapeyron-slope indicates that the phase transition is exothermic and it is predicted that the rehydrogenation of the high pressure orthorhombic phase would be easier due to its lower enthalpy.

Introduction

Ammonia borane [1,2] is one of the most promising materials for on-board hydrogen storage due to its high energy storage efficiency (19.6 wt% of hydrogen). Dehydrogenation of ammonia borane below 200 °C proceeds in two steps [2,3]:

$$n\,NH_3BH_3\,(solid) \rightarrow [NH_2BH_2]_n(solid) + nH_2(gas) \quad \text{at } 100^\circ C \tag{1}$$

$$[NH_2BH_2]_n(solid) \rightarrow [N_3B_3H_6]_{n/3}(liquid) + nH_2(gas) \quad \text{at } 160^\circ C \tag{2}$$

These two decomposition steps, which take place at mild conditions, are favorable for on-board applications. Total of

* *Corresponding author*. Center for High Pressure Science and Technology Advanced Research, Jilin University, Changchun 120013, China.
E-mail address: chenj@fiu.edu (J. Chen).

http://dx.doi.org/10.1016/j.ijhydene.2014.03.070

Table 1 – Selected Raman modes of ammonia borane (compared with previous studies).

	Yu et al. [23]		Xie et al. [26]		This work					
					22 °C		60 °C		100 °C	
	Peak position (cm^{-1})	Pressure (GPa)	Peak position (cm^{-1})	Pressure (GPa)	Peak position (cm^{-1})	Pressure (GPa)	Peak position (cm^{-1})	Pressure (GPa)	Peak position (cm^{-1})	Pressure (GPa)
N–H stretching sym	3247	0.7	3253	0	3245	0.7	3248	0.7	3246	0.77
N–H stretching asym.	3308	0.7	3319	0	3308	0.7	3311	0.7	3311	0.77
^{11}B–N stretching	795	0.7	783	0	793	0.7	798	0.7	792	0.77
^{10}B–N stretching	815	0.7	798	0	810	0.7	813	0.7	806	0.77
B–H stretching sym	2293	0.7	2280	0	2289	0.7	2290	0.7	2287	0.77
B–H stretching asym. overtone	2322	0.7			2335	1.05	2333	0.7	2334	0.77
B–H stretching asym.	2397	0.7	2376	0	2379	0.7	2374	0.7	2388	0.77

13 wt% hydrogen is released in these two steps exceeding DOE ultimate target of hydrogen storage capacity (7.5 wt% H) [4].

However, low decomposition rate, undesired volatile products as well as low or non-rechargeability hinder ammonia borane from on-board application. Many approaches, such as hydrolysis [5–8], nano confinement [9–17], acid initiation [18], and ionic liquids [7] were able to increase the decomposition rate or decrease the decomposition temperature. Alkali metal substitution of one hydrogen atom in ammonia borane generates alkali metal amidoboranes, MNH_2BH_3, which also have improved hydrogen desorption performance [5].

Ammonia borane has been intensively studied by IR and Raman spectroscopy [19–28], X-Ray diffraction [29–32], NMR

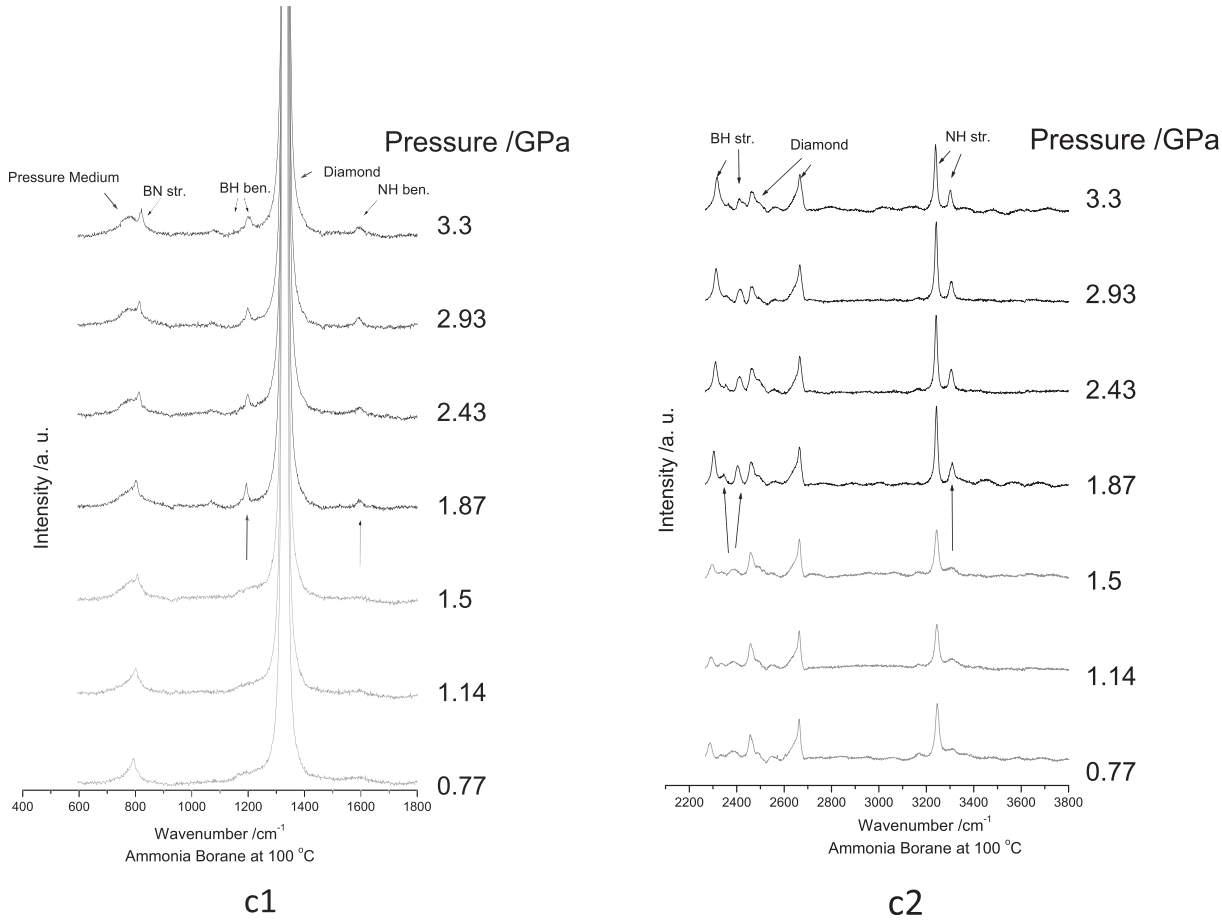

Fig. 1 – Raman spectra of ammonia borane at different pressures with pressure medium. Gray lines refer to I4mm phase, black lines refer to $Cmc2_1$ phase; a1–a2, b1–b2 and c1–c2 are at 20 °C, 60 °C and 100 °C, respectively (a1 and a2 represents first and second ranges of Raman spectra, similar with b1, b2, c1 and c2). In each figure, the pressure of the Raman spectrum was increased stepwise from bottom to top.

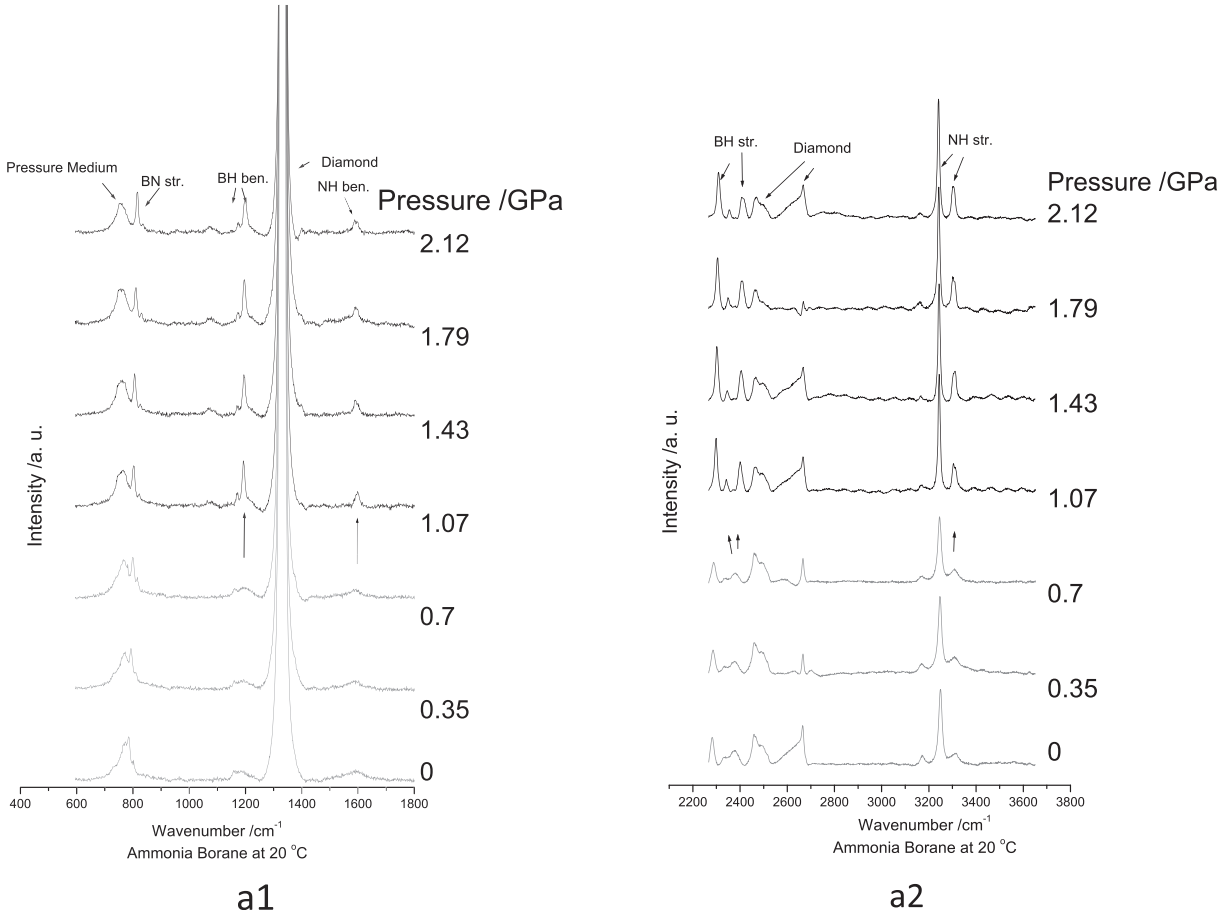

Fig. 1 – (*continued*).

[15,33–35], theoretical computation [31,36–39], neutron scattering or diffraction [37,40–42], and anelastic spectroscopy [43], etc. High pressure study has also drawn great attention recently [23,24,26–28,44]. Pressure dependence of the first and second decomposition temperature was studied by Nylen et al. [45] using Raman spectroscopy, showing that decomposition temperatures of the first two steps increase with pressure. Interactions between decomposed ammonia borane and hydrogen at high pressure [25,27,28] have been studied, but directly reversed reaction of the thermolysis has not been observed. Pressure and temperature induced phase transitions of ammonia borane were also studied extensively to investigate its stability with pressure and temperature. At ambient pressure, low temperature studies show that ammonia borane transforms from orthorhombic to tetragonal structure at ~225 K [22,32,34,40,43,46–49]. At room temperature, there are several phase transitions of ammonia borane at ~0.8, 2, 5, 8, 10 and 12 GPa, which were observed by Raman spectroscopy studies [20,21,23,26]. X-ray diffraction studies [29–31,44] confirmed a first-order phase transitions (I4mm to $Cmc2_1$) at ~1 GPa, a second-order phase transition at 5 GPa, and another first-order phase transition ($Cmc2_1$ to $P2_1$) at ~12.9 GPa. A new phase at 4 GPa and 450 K was also observed using the X-ray study by Chen et al [30]. A later synchrotron X-ray diffraction (XRD) study observed a similar new phase at 140 °C and ~6 GPa [50]. Based on their reported XRD patterns, those two observations are likely to be the same phase.

The first-order phase transition (*I4mm* to $Cmc2_1$) is very interesting since it occurs at relatively low pressure (~1 GPa at room temperature). And it is expected to influence the hydrogen storage properties when we apply high pressure over the phase boundary. Ammonia borane's thermodynamic properties of this transition are also very important for hydrogen storage study. In this paper, this phase transition (*I4mm* to $Cmc2_1$) was studied at high pressure and elevated temperature up to 100 °C using Raman spectroscopy and synchrotron X-ray diffraction, and the thermodynamic properties of this transition are also evaluated.

Experiment

The ammonia borane sample, NH_3BH_3 (99% pure), was purchased from Sigma–Aldrich Co. and used without any additional purification. The sample was loaded into a Mao-Bell type diamond anvil cell (DAC) with 400 μm culet anvils. Sample chamber was a hole in the 302 stainless steel gasket 100–150 μm in diameter and 60–80 μm thick foil. Ruby fluorescence method with temperature correction [51,52] was used to determine the pressure inside the DAC. In one group of *in situ* Raman measurements, a mixture of ethanol and methanol (1:4 volume ratio) was used to compare the influence of stress and interaction between sample and pressure medium. In another group of *in situ* Raman measurement, no

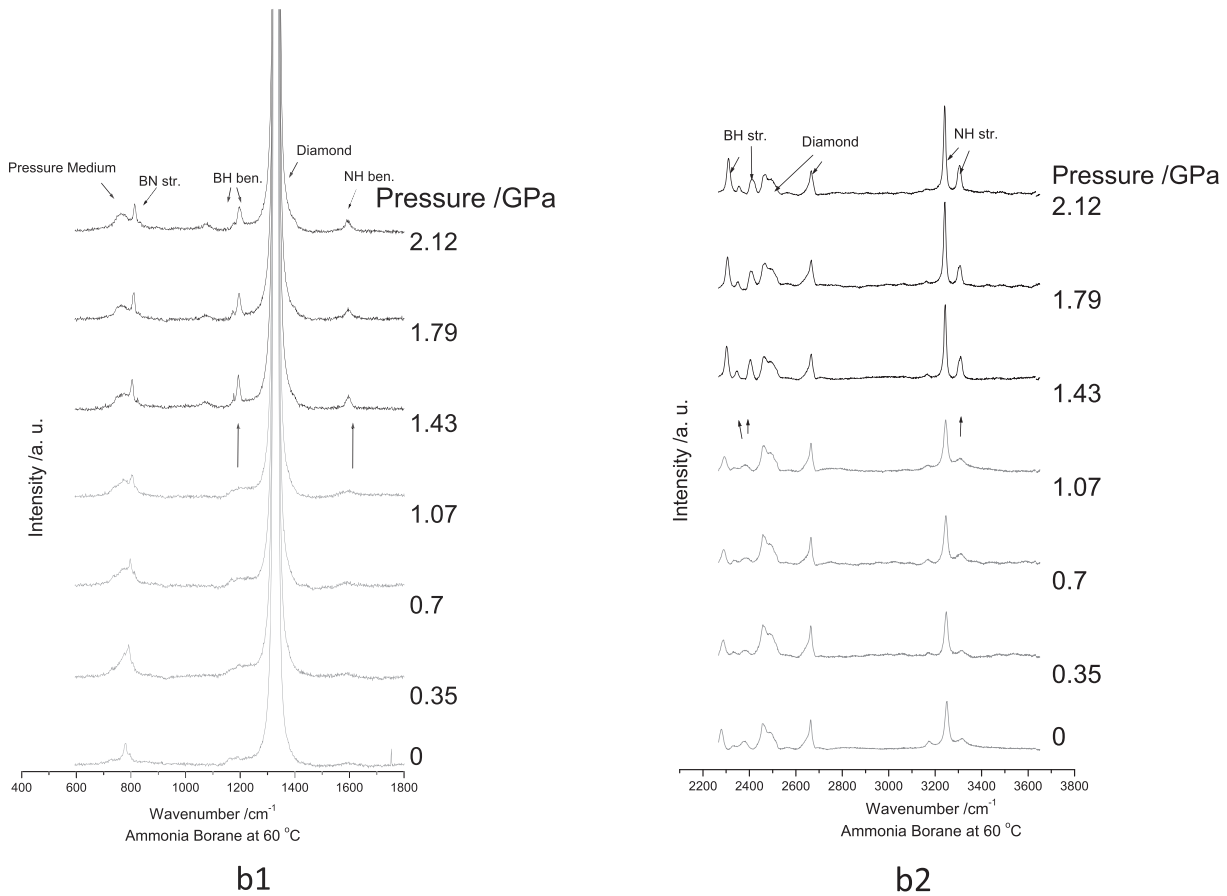

Fig. 1 – (*continued*).

pressure medium was used. In the following XRD experiments, no pressure medium was used.

High temperature in the DAC was achieved using an external band heater surrounding the cells and the temperature was controlled using a thermal controller. Two K-type thermocouples were used for temperature measurements: the first one was positioned near the sample chamber in contact with one of the diamond anvils to measure the sample temperature, and the second one was positioned near the heater to receive quick feedback for controlling the temperature within small fluctuations (±2 °C). As well, the cell was isolated by several layers of asbestos paper to improve heating efficiency. The 541.5 nm line of Spectra-Physics Air-Cooled Argon-Ion Laser was used to excite the sample. The scattering signals were collected with an exposure time of 2 min using a high throughput holographic imaging spectrometer consisting of volume transmission grating, holographic notch filter and thermoelectrically cooled CCD detector (Andor). Raman spectra were recorded by back-scattering configuration.

Three separate high pressure experiments were conducted at 20 °C, 60 °C and 100 °C. In each experiment, the cell was first closed with minimal pressure (near ambient pressure) and externally heated to the desired temperature. After the desired temperature was stabilized, the pressure was increased from minimal pressure to maximum pressure stepwise with an interval of ~0.35 GPa and then decreased back to near ambient pressure. At each step, pressure was carefully adjusted to a certain value with ~0.35 GPa interval and held for a few minutes before Raman measurement.

Results and discussion

To make comparisons, the first group of our experiments of Raman spectroscopy were conducted with pressure medium (a 1:4 volume ratio mixture of ethanol and methanol) and the second group were just repeated but without pressure medium. Each of the Raman spectra was collected by one measurement but divided into two parts by the Andor Raman system: the first range from ~600 cm^{-1} to ~1800 cm^{-1} and the second range from ~2200 cm^{-1} to ~3700 cm^{-1}. The Raman spectra were analyzed by 5 regions: NH stretching region (in the second range: 3150 cm^{-1}–3350 cm^{-1}), BH stretching region (in the second range: 2250 cm^{-1}–2550 cm^{-1}), BN stretching region (in the first range: 700 cm^{-1}–1000 cm^{-1}), BH bending region (in the first range: 1150 cm^{-1}–1300 cm^{-1}), NH bending region (in the first range: 1450 cm^{-1}–1700 cm^{-1}). In Table 1, the Raman spectra at (Fig. 1a1 and a2) are summarized and compared with those from previous studies [20,21,23,26]. For comparison, we put the Raman spectra measured at different pressures but the same temperature in the same figure. For example, Fig. 1a1 shows the first range Raman spectra of ammonia borane with pressure medium at room temperatures for each pressures during compression and decompression.

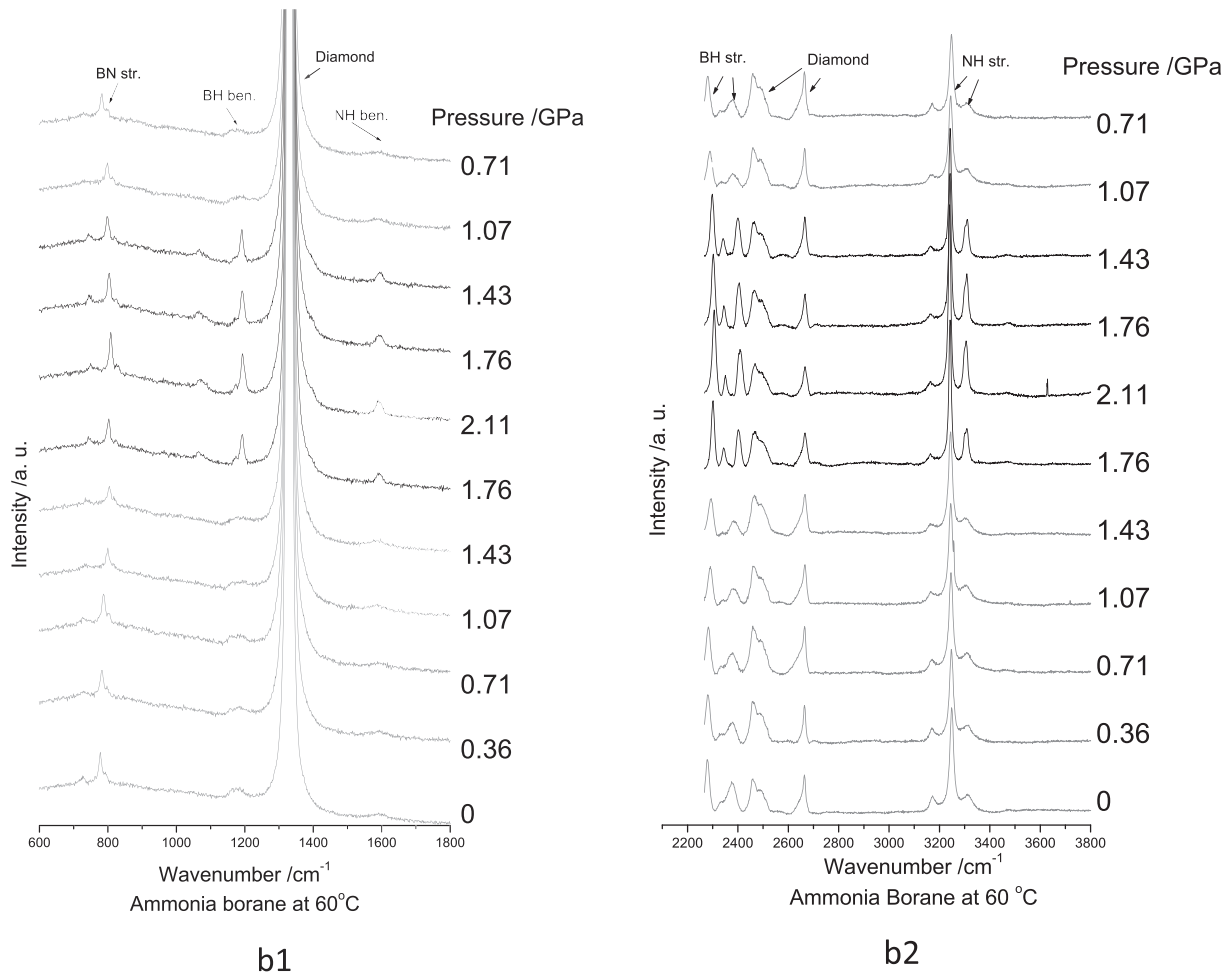

Fig. 2 – Raman spectra of ammonia borane at different pressures without pressure medium. Gray lines refer to I4mm phase, black lines refer to Cmc2$_1$ phase; a1–a2, b1–b2 and c1–c2 are at 20 °C, 60 °C and 100 °C, respectively (a1 and a2 represents first and second ranges of Raman spectra, similar with b1, b2, c1 and c2). In each figure, the pressure of the Raman spectrum was increased stepwise from bottom to top.

Similarly, Fig. 1a2 shows that of the second range. As declared before, the first range and the second range for each Raman spectroscopy are from the same measurement.

Fig. 1 shows the Raman spectra of ammonia borane with pressure medium at different pressures and temperatures. Upon compression to ~1.07 GPa, most peaks of ammonia borane become higher and sharper. As well, there are two peak splittings which are asymmetric N–H stretching mode and asymmetric B–H stretching mode. These changes indicate a phase transition and the transition pressure is consistent with that of the first-order phase transition (*I4mm* to *Cmc2*$_1$) which was detected by XRD studies [29–31,44]. Fig. 1b1, b2, c1 and c2 shows the phase transition pressure increases to ~1.43 GPa and ~1.87 GPa at 60 °C and 100 °C, respectively.

At each temperature, pressure raising makes most of the peaks shift towards higher wavenumbers (the positive pressure dependence) except that of N–H stretching and N–H bending modes (the negative pressure dependence). The negative pressure dependences of the N–H stretching and N–H bending modes are due to dihydrogen bonding (B–H···H–N) effect [20]. In another comparative experiment without pressure medium, although the phase transition pressure shows small hysteresis (less than 0.3 GPa) compared to that with pressure medium (see Fig. 2), we did not find any obvious difference between the Raman spectra of the two experiments. The spectroscopic consistency between the two experiments indicates that there is no reaction between the sample and the pressure medium. In the experiment without pressure medium, Raman spectra were also recorded during a slow pressure decompression. At each temperature, the phase transitions are all reversible within small pressure hysteresises. The small pressure hysteresis also indicates that ammonia borane is reasonably soft to produce a quasi-hydrostatic condition [23].

To make comparison with previously studied crystalline phase transition, we also conducted synchrotron XRD experiment at room temperature. The lower pressure pattern of synchrotron X-ray diffraction (Fig. 3) is identified to be the *I4mm* phase, the first-order phase transition (*I4mm* to *Cmc2*$_1$) of ammonia borane occurred after pressure rising to ~0.7 GPa. Due to the quasi-hydrostatic status and ruby system uncertainty, our transition pressure detected by XRD was lower than that was detected by our Raman spectra (between 0.7 and 1.2 GPa) or previous studies [29–31,44] (1.1–1.3 GPa). Our XRD

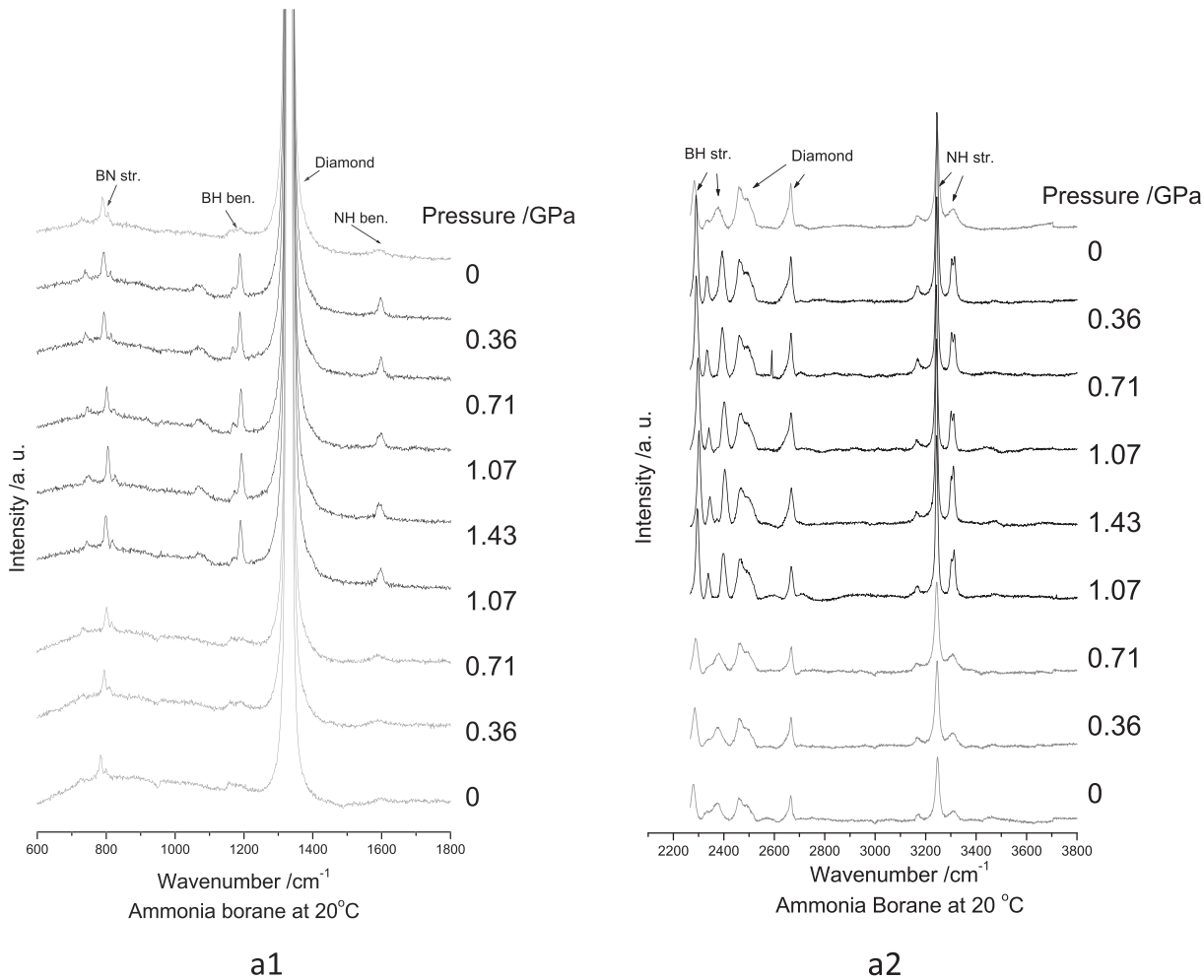

Fig. 2 – (*continued*).

pattern shows the high pressure phase $Cmc2_1$ is stable from ~0.7 GPa up to ~10 GPa without further phase transition. When the pressure increased to ~13.7 GPa, ammonia borane transformed to a new phase, which was identified to be $P2_1$ as previous reported [44].

The stability fields of *I4mm* and $Cmc2_1$ phases are summarized in Fig. 4. The phase $Cmc2_1$ from the experiment without pressure medium was transformed back to *I4mm* phase at lower pressure during decompression compared to that during pressure rising, indicating the phase transition is sluggish at these temperatures. The difference in the transition pressure during compression and decompression becomes smaller at higher temperatures as the transition kinetics getting faster at higher temperature. The phase boundary that was identified from the experiment with pressure medium is not marked in this figure, but it falls in between the two boundaries defined above. All these data consistently indicate that the equilibrium phase boundary between the *I4mm* phase and $Cmc2_1$ phase has a positive slope and locates within the area between compression boundary and decompression boundary. This result disagrees with previous multi-anvil X-ray diffraction study [30] which reported a negative slopped phase boundary. It is likely due to a possible confusion between diffraction peaks from the high pressure phase ammonia borane and its surrounding materials, since the sample position would be likely to shift at higher pressure during the multi-anvil press.

The Clausius–Clapeyron relation gives the slope of the tangent to the phase boundary. Thermodynamically,

$$dP/dT = \Delta S/\Delta V$$

where, P is the pressure, T is the temperature, dP/dT is the slope of tangent to the coexistence curve at any point, ΔS is the specific entropy change during phase transition, and ΔV is the specific volume change during phase transition. Therefore,

$$\Delta S = \Delta V * (dP/dT)$$

Our experiment indicates that dP/dT for the I4mm and $Cmc2_1$ phase boundary is positive. As ΔV is always negative upon compression ($\Delta V < 0$), ΔS is therefore negative,

$$\Delta S = \Delta V * (dP/dT) < 0$$

During a phase transition, $\Delta G = 0$, therefore, the enthalpy change for the transition,

$$\Delta H = \Delta G + T\Delta S = T\Delta S < 0$$

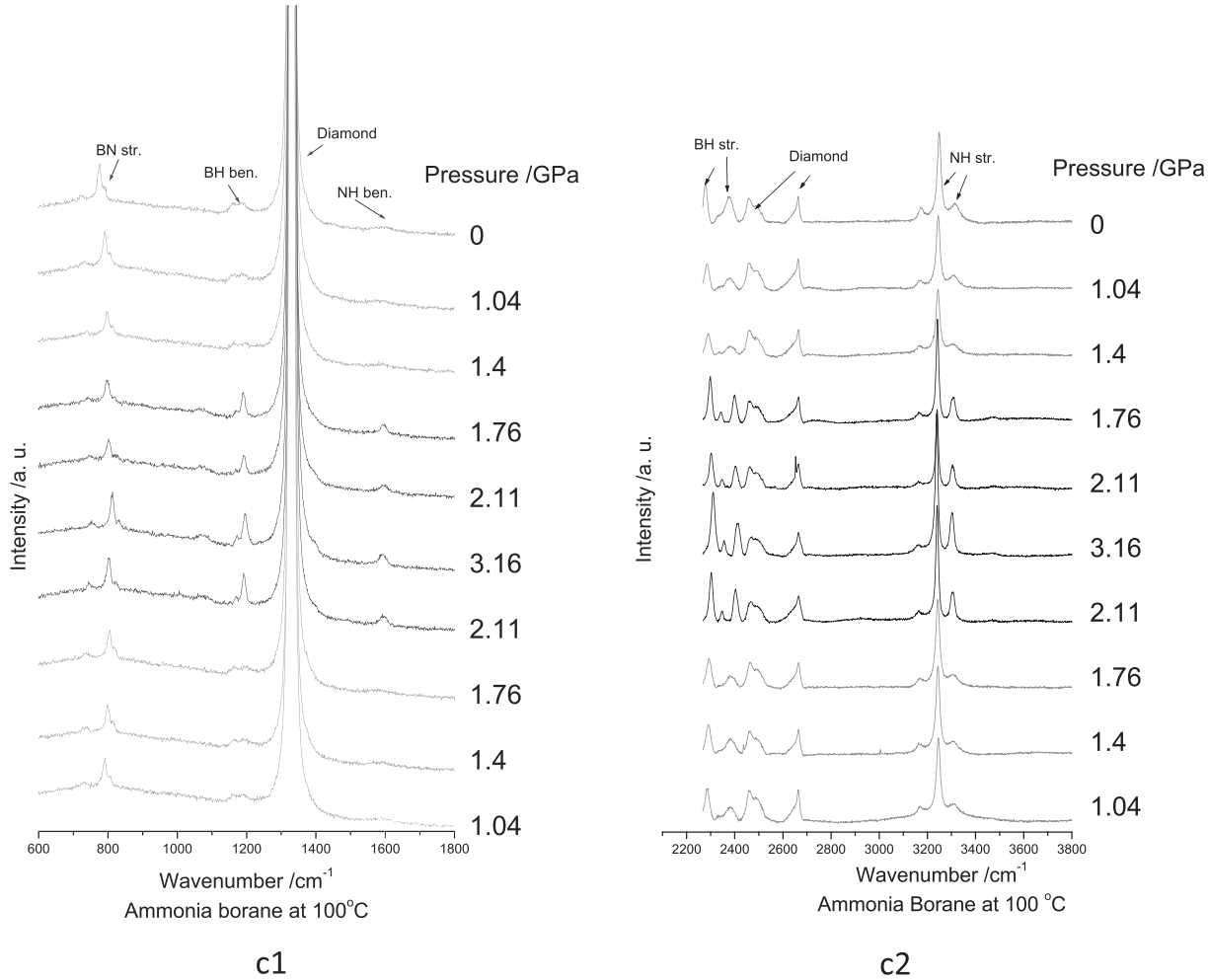

Fig. 2 – (*continued*).

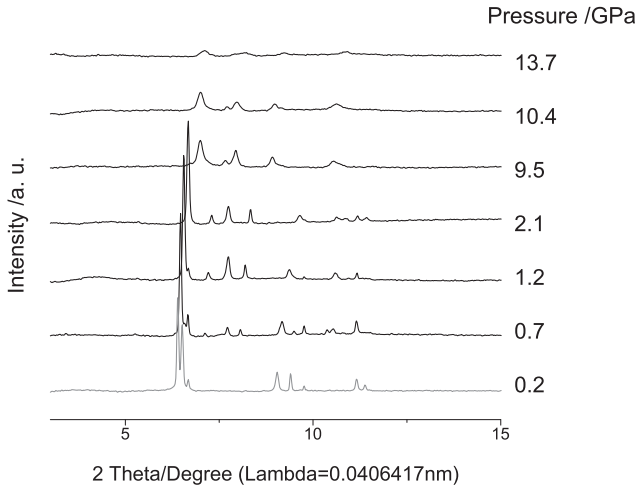

Fig. 3 – Synchrotron X-Ray diffraction patterns of ammonia borane at room temperature (gray: I4mm, black: $Cmc2_1$) during compression run.

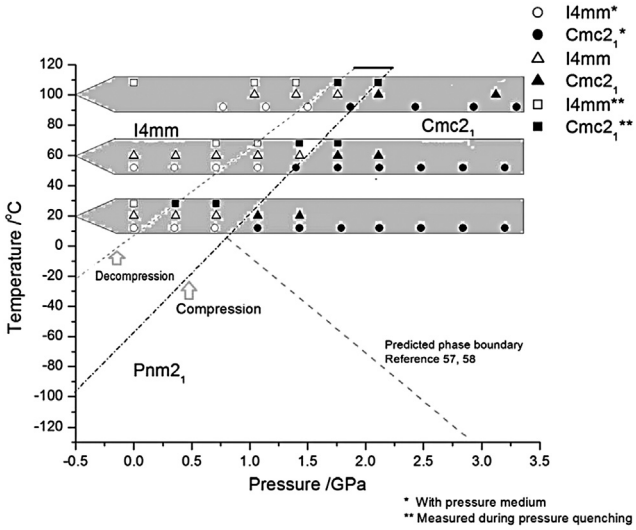

Fig. 4 – Phase boundary between I4mm and $Cmc2_1$ phases of ammonia borane by Raman spectroscopy. All the data within a horizontal shaded area are taken at the same temperature labeled on the left, but plotted separately for easy recognition.

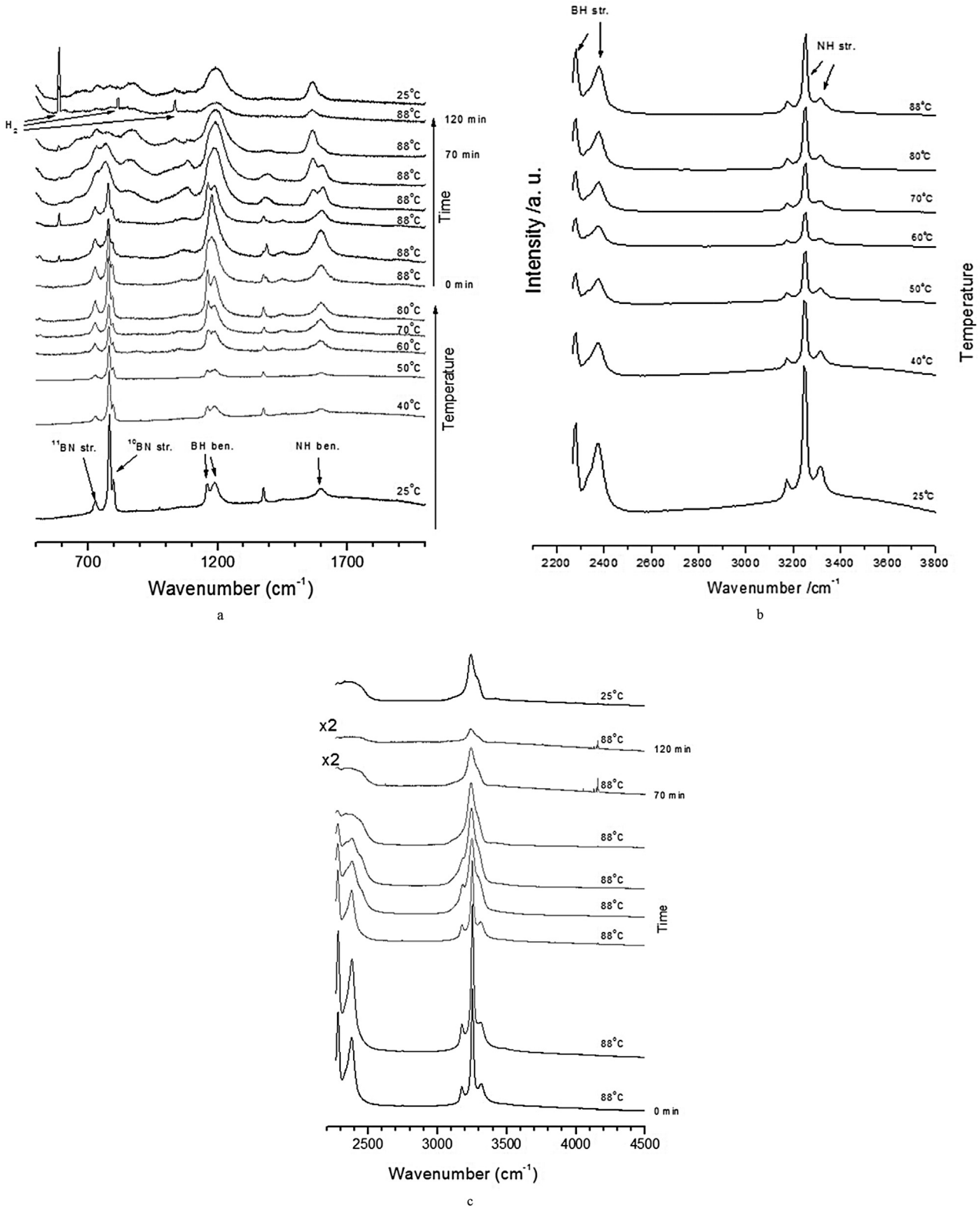

Fig. 5 – Raman spectra of ammonia borane during decomposition at ambient pressure. a, first range of Raman spectra, 500 cm^{-1}–2000 cm^{-1}, as a function of temperature (the first six spectra from bottom) and a function of time at a constant temperature of 88 °C (rest of the spectra on the top); b, second range of Raman spectra, 2200 cm^{-1}–4500 cm^{-1}, as a function of temperature (increasing from bottom to top); c, second range of Raman spectra (continue), 2200 cm^{-1}–4500 cm^{-1}, as a function of time (from bottom to top) at a constant temperature of 88 °C.

where: ΔG is the specific Gibbs free energy change during the phase transition.

The above analysis indicates that the $Cmc2_1$ phase has lower enthalpy than that of *I4mm* phase. Therefore the pressure-induced phase transition from *I4mm* to $Cmc2_1$ is exothermic. As previously reported [3], one of the barriers for rehydrogenation of ammonia borane after the first two step decompositions is the high exothermic enthalpies during the decompositions. The current study indicates that the orthorhombic phase of ammonia borane has lower enthalpy than that of tetragonal phase. If we assume decomposition from the orthorhombic phase yields the same products as that from the tetragonal phase, the decomposition of the orthorhombic phase will be less exothermic. Therefore rehydrogenation from the decomposed product into the orthorhombic phase at high pressure may become easier. However, it is difficult to quantify the enthalpy of the high pressure transition to give a quantitative estimation of how much easier such a rehydrogenation is.

The extrapolated I4mm–$Cmc2_1$ phase boundary in low temperature region crosses the temperature axis (at ambient pressure) in a region between −30 °C and −120 °C, predicting a low temperature phase transition at ambient pressure (as shown in Fig. 4). This transition temperature matches well with previous low temperature structural phase transition studies (I4mm to $Pnm2_1$) at ~−48 °C [22,34,40,43,46–49]. Fig. 4 also shows a phase boundary between the $Cmc2_1$ phase and $Pnm2_1$ phase predicted by previous low temperature high pressure Raman studies (the gray dashed line in Fig. 4) [53,54].

We didn't find any features of decomposition from our high pressure Raman spectra of ammonia borane at elevated temperature up to 100 °C and elevated pressures. However, our additional experiment proved that the ammonia borane could be decomposed below 100 °C, even within 2 h at 88 °C at ambient pressure, as shown in Fig. 5. The DAC seals ammonia borane in a limited space, which increased the decomposition temperature. This result is consistent with previous reports [45]. On the other hand, the difficulties in the decomposition may also indicate an easier reversible rehydrogenation.

Conclusion

The Raman spectroscopy study shows that the first-order phase transition from *I4mm* to $Cmc2_1$ in ammonia borane is reversible with a small hysteresis, while the phase boundary shifts towards higher pressure with a positive Clapeyron-slope at higher temperature. The positive Clapeyron-slope indicates that the phase transition is exothermic. This result indicates that the rehydrogenation of the high pressure orthorhombic phase would be easier due to its lower enthalpy compared to that of ambient pressure tetragonal phase.

Acknowledgment

This work was supported by the U.S. Department of Energy, Office of Science, Office of Basic Energy Sciences under Award No. DE-FG02-07ER46461. The synchrotron XRD study was conducted at Beamline X17C, National Synchrotron Light Source (NSLS), Brookhaven National Lab (BNL) with the help of the beamline scientist, Dr. Zhiqiang Chen. The high pressure facility at NSLS is supported by COMPRES, the Consortium for Materials Properties Research in Earth Sciences under NSF Cooperative Agreement EAR 06-49658. We thank EFree, an Energy Frontier Research Center funded by the US DOE, Office of Science, and Office of Basic Energy Sciences under Award DESC0001057 for partial personnel support. We would like to thank Dr. S. Saxena for his useful discussions.

REFERENCES

[1] Shore SG, Parry RW. The crystalline compound ammonia-borane, 1 H_3NBH_3. J Am Chem Soc 1955;77(22):6084–5.
[2] Hu MG, Geanangel RA, Wendlandt WW. The thermal decomposition of ammonia borane. Thermochim Acta 1978;23(2):249–55.
[3] Wolf G, Baumann J, Baitalow F, Hoffmann FP. Calorimetric process monitoring of thermal decomposition of B–N–H compounds. Thermochim Acta 2000;343(1–2):19–25.
[4] DOE targets for onboard hydrogen storage systems for light-duty vehicles. US Department of Energy, Office of Energy Efficiency and Renewable Energy and The FreedomCAR and Fuel Partnership; Sep. 2009. revision 4.0:9.
[5] Xiong Z, Yong CK, Wu G, Chen P, Shaw W, Karkamkar A, et al. High-capacity hydrogen storage in lithium and sodium amidoboranes. Nat Mater 2008;7(2):138–41.
[6] Chandra M, Xu Q. Dissociation and hydrolysis of ammonia–borane with solid acids and carbon dioxide: an efficient hydrogen generation system. J Power Sources 2006;159(2):855–60.
[7] Bluhm ME, Bradley MG, Butterick R, Kusari U, Sneddon LG. Amineborane-based chemical hydrogen storage: enhanced ammonia borane dehydrogenation in ionic liquids. J Am Chem Soc 2006;128(24):7748–9.
[8] Denney MC, Pons V, Hebden TJ, Heinekey DM, Goldberg KI. Efficient catalysis of ammonia borane dehydrogenation. J Am Chem Soc 2006;128(37):12048–9.
[9] Gutowska A, Li L, Shin Y, Wang CM, Li XS, Linehan JC, et al. Nanoscaffold mediates hydrogen release and the reactivity of ammonia borane. Angew Chem Int Ed 2005;44(23):3578–82.
[10] Nielsen TK, Polanski M, Zasada D, Javadian P, Besenbacher F, Bystrzycki J, et al. Improved hydrogen storage kinetics of nanoconfined $NaAlH_4$ catalyzed with $TiCl_3$ nanoparticles. ACS Nano 2011;5(5):4056–64.
[11] Gadipelli S, Ford J, Zhou W, Wu H, Udovic TJ, Yildirim T. Nanoconfinement and catalytic dehydrogenation of ammonia borane by magnesium-metal–organic-framework-74. Chem Eur J 2011;17(22):6043–7.
[12] Fetz M, Gerber R, Blacque O, Frech CM. Hydrolysis of ammonia borane catalyzed by aminophosphine-stabilized precursors of rhodium nanoparticles: ligand effects and solvent-controlled product formation. Chem Eur J 2011;17(17):4732–6.
[13] Zhao J, Shi J, Zhang X, Cheng F, Liang J, Tao Z, et al. A soft hydrogen storage material: poly(methyl acrylate)-confined ammonia borane with controllable dehydrogenation. Adv Mater 2010;22(3):394–7.
[14] Li Z, Zhu G, Lu G, Qiu S, Yao X. Ammonia borane confined by a metal–organic framework for chemical hydrogen storage: enhancing kinetics and eliminating ammonia. J Am Chem Soc 2010;132(5):1490–1.
[15] Wang L-Q, Karkamkar A, Autrey T, Exarhos GJ. Hyperpolarized 129Xe NMR investigation of ammonia borane in mesoporous silica. J Phys Chem C 2009;113(16):6485–90.

[16] Kim H, Karkamkar A, Autrey T, Chupas P, Proffen T. Determination of structure and phase transition of light element nanocomposites in mesoporous silica: case study of NH_3BH_3 in MCM-41. J Am Chem Soc 2009;131(38):13749–55.

[17] Sepehri S, Feaver A, Shaw WJ, Howard CJ, Zhang Q, Autrey T, et al. Spectroscopic studies of dehydrogenation of ammonia borane in carbon cryogel. J Phys Chem B 2007;111(51):14285–9.

[18] Stephens FH, Baker RT, Matus MH, Grant DJ, Dixon DA. Acid initiation of ammonia–borane dehydrogenation for hydrogen storage. Angew Chem Int Ed 2007;46(5):746–9.

[19] Smith J, Seshadri KS, White D. Infrared spectra of matrix isolated BH_3–NH_3, BD_3–ND_3, and BH_3–ND_3. J Mol Spectrosc 1973;45(3):327–37.

[20] Custelcean R, Dreger ZA. Dihydrogen bonding under high pressure: a Raman study of BH_3NH_3 molecular crystal. J Phys Chem B 2003;107(35):9231–5.

[21] Trudel S, Gilson DFR. High-pressure Raman spectroscopic study of the ammonia–borane complex. Evidence for the dihydrogen bond. Inorg Chem 2003;42(8):2814–6.

[22] Hess NJ, Bowden ME, Parvanov VM, Mundy C, Kathmann SM, Schenter GK, et al. Spectroscopic studies of the phase transition in ammonia borane: Raman spectroscopy of single crystal NH_3BH_3 as a function of temperature from 88 to 330 K. J Chem Phys 2008;128(034508).

[23] Lin Y, Mao WL, Drozd V, Chen J, Daemen LL. Raman spectroscopy study of ammonia borane at high pressure. J Chem Phys 2008;129(234509).

[24] Lin Y, Mao WL, Mao H-k. Storage of molecular hydrogen in an ammonia borane compound at high pressure. Proc Natl Acad Sci 2009;106(20):8113–6.

[25] Wang S, Mao WL, Autrey T. Bonding in boranes and their interaction with molecular hydrogen at extreme conditions. J Chem Phys 2009;131(144508).

[26] Xie S, Song Y, Liu Z. In situ high-pressure study of ammonia borane by Raman and IR spectroscopy. Can J Chem 2009;87:1235–47.

[27] Chellappa Raja S, Autrey T, Somayazulu Maddury, Struzhkin Viktor V, Hemley Russell J. High-pressure hydrogen interactions with polyaminoborane and polyiminoborane. ChemPhysChem 2010;11:93–6.

[28] Chellappa Raja S, Somayazulu Maddury, Struzhkin Viktor V, Autrey Thomas, Hemley Russell J. Pressure-induced complexation of NH_3BH_3–H_2. J Chem Phys 2009;131(224515).

[29] Hoon CF, Reynhardt EC. Molecular dynamics and structures of amine boranes of the type R_3N BH_3. I. X-ray investigation of H_3N BH_3 at 295 K and 110 K. J Phys C Solid State Phys 1983;16(32):6129.

[30] Chen J, Couvy H, Liu H, Drozd V, Daemen LL, Zhao Y, et al. In situ X-ray study of ammonia borane at high pressures. Int J Hydrogen Energy 2010;35(20):11064–70.

[31] Filinchuk Y, Nevidomskyy AH, Chernyshov D, Dmitriev V. High-pressure phase and transition phenomena in ammonia borane NH_3BH_3 from x-ray diffraction, Landau theory, and ab initio calculations. Phys Rev B – Condens Matter 2009;79(21):214111.

[32] Bowden ME, Gainsford GJ, Robinson WT. Room-temperature structure of ammonia borane. Aust J Chem 2007;60(3):149–53.

[33] Penner GH, Chang YCP, Hutzal J. A deuterium NMR spectroscopic study of solid BH_3NH_3. Inorg Chem 1999;38(12):2868–73.

[34] Gunaydin-Sen O, Achey R, Dalal NS, Stowe A, Autrey T. High resolution 15N NMR of the 225 K phase transition of ammonia borane (NH_3BH_3): mixed order–disorder and displacive behavior. J Phys Chem B 2007;111(4):677–81.

[35] Reynhardt EC, Hoon CF. Molecular dynamics and structures of amine boranes of the type R_3N BH_3. II. NMR investigation of H_3N BH_3. J Phys C Solid State Phys 1983;16(32):6137.

[36] Wang L, Bao K, Meng X, Wang X, Jiang T, Cui T, et al. Structural and dynamical properties of solid ammonia borane under high pressure. J Chem Phys 2011;134(024517).

[37] Hess NJ, Schenter GK, Hartman MR, Daemen LL, Proffen T, Kathmann SM, et al. Neutron powder diffraction and molecular simulation study of the structural evolution of ammonia borane from 15 to 340 K. J Phys Chem A 2009;113(19):5723–35.

[38] Lochan Rohini C, -Gordon Martin Head. Computational studies of molecular hydrogen binding affinities: the role of dispersion forces, electrostatics, and orbital interactions. Phys Chem Chem Phys 2006;2006(8):1357–70.

[39] Dillen J, Verhoeven P. The end of a 30-year-old controversy? A computational study of the B–N stretching frequency of BH_3–NH_3 in the solid state. J Phys Chem A 2003;107(14):2570–7.

[40] Hess NJ, Hartman MR, Brown CM, Mamontov E, Karkamkar A, Heldebrant DJ, et al. Quasielastic neutron scattering of $-NH_3$ and $-BH_3$ rotational dynamics in orthorhombic ammonia borane. Chem Phys Lett 2008;459(1–6):85–8.

[41] Brown CM, Jacques TL, Hess NJ, Daemen LL, Mamontov E, Linehan JC, et al. Dynamics of ammonia borane using neutron scattering. Phys B Condens Matter 2006;385–386(Part 1):266–8.

[42] Klooster WT, Koetzle TF, Siegbahn PEM, Richardson TB, Crabtree RH. Study of the N–H···H–B dihydrogen bond including the crystal structure of BH_3NH_3 by neutron diffraction. J Am Chem Soc 1999;121(27):6337–43.

[43] Paolone A, Palumbo O, Rispoli P, Cantelli R, Autrey T. Hydrogen dynamics and characterization of the tetragonal-to-orthorhombic phase transformation in ammonia borane. J Phys Chem C 2009;113(14):5872–8.

[44] Lin Y, Ma H, Matthews CW, Kolb B, Sinogeikin S, Thonhauser T, et al. Experimental and theoretical studies on a high pressure monoclinic phase of ammonia borane. J Phys Chem C 2012;116(3):2172–8.

[45] Johanna Nylén, Toyoto Sato, Emmanuel Soignard, Yarger Jeffery L, Emil Stoyanov, Ulrich Häussermann. Thermal decomposition of ammonia borane at high pressures. J Chem Phys 2009;131(104506).

[46] Lippert EL, Lipscomb WN. The structure of H_3NBH_3. J Am Chem Soc 1956;78(2):503–4.

[47] Cho H, Shaw WJ, Parvanov V, Schenter GK, Karkamkar A, Hess NJ, et al. Molecular structure and dynamics in the low temperature (orthorhombic) phase of NH_3BH_3. J Phys Chem A 2008;112(18):4277–83.

[48] Paolone A, Palumbo O, Rispoli P, Cantelli R, Autrey T, Karkamkar A. Absence of the structural phase transition in ammonia borane dispersed in mesoporous silica: evidence of novel thermodynamic properties. J Phys Chem C 2009;113(24):10319–21.

[49] Yang JB, Lamsal J, Cai Q, James WJ, Yelon WB. Structural evolution of ammonia borane for hydrogen storage. Appl Phys Lett 2008;92(9):091916.

[50] Nylen J, Eriksson L, Benson D, Haussermann U. Characterization of a high pressure, high temperature modification of ammonia borane (BH_3NH_3). J Chem Phys 2013;139(05450).

[51] Rekhi S, Dubrovinsky LS, Saxena SK. Temperature-induced ruby fluorescence shifts up to a pressure of 15 GPa in an externally heated diamond anvil cell. High Temp High Press 1999;31(3):299–305.

[52] Mao HK, Xu J, Bell PM. Calibration of the ruby pressure gauge to 800 kbar under quasi-hydrostatic conditions. J Geophys Res 1986;91(B5):4673–6.

[53] Liu A, Song Y. In situ high-pressure and low-temperature study of ammonia borane by Raman spectroscopy. J Phys Chem C 2011;116(3):2123–31.

[54] Najiba S, Chen J, Drozd V, Durygin A, Sun Y. Tetragonal to orthorhombic phase transition of ammonia borane at low temperature and high pressure. J Appl Phys 2012;111(11):112618.